J. Nanoanalysis., 10(1): 415-427, Winter 2023

RESEARCH ARTICLE

Theoretical investigation of optical properties of Aluminum zig-zag thin films

Maryam Gholizadeh Arashti [*,1], ***Mahsa Fakharpour*** [2]

[1] *Department of Physics, Yadegar-e-Imam Khomeini (RAH) Shahre Rey Branch, Islamic Azad University, Tehran, Iran*

[2] *Department of Physics, Maybod Branch, Islamic Azad University, Maybod, Iran.*

ARTICLE INFO

Article History:
Received 2020-08-19
Accepted 2020-10-29
Published 2023-02-15

Keywords:
Reflectance,
Transfer matrix,
Zig-zag nanostructure,
Linearly polarized light,
Bragg phenomenon

ABSTRACT

The transfer matrix method was applied to model the reflection and transmission co-polarization spectra of zig-zag aluminum thin films by different arm numbers and lengths and the optical spectra of the zig-zag nanostructures for both s- and p-polarized lights were obtained at different incident angles. According to the results, for the s-polarized incident light, the transmission reduces and the reflection increases by incident angle. For the p- polarized light, the reflection is reduced for the incident directions near the Bruster's angle and the transmission almost remains constant. The numbers of Bragg peaks via arm number were also considered for s-polarized light at the 60° incident angle. The results determined four arms as the period of zig-zag structure. Besides, the red and blue shifts were observed for the wavelengths smaller and greater than 550 nm, respectively. At last, no Bragg peak was observed for p-polarized light at all incident angles.

How to cite this article
Gholizadeh-Arashti M., Fakharpour M., Theoretical investigation of optical properties of Aluminum zig-zag thin films. J. Nanoanalysis., 10(1): 415-427, Winter 2023. DOI: 10.22034/jna.2020.1907296.1226

INTRODUCTION

In the recent years, the metal-dielectric composite layers have been increasingly regarded and their structural, optical and electrical properties have been widely studied, both experimentally and theoretically. Among the metallic elements used in these composite layers, the aluminum (Al) has received special attentions due to its simple thin film preparation process [1, 2]. The electrical conductivity near its bulk value [3] also introduces it as an ideal element for the optoelectronic devices production [4, 5]. The physical properties of Al thin films are sensitively related to their microstructures [6, 7], so it may be manipulated [8-10] controllably. The plasmonic properties of $Al@Al_2O_3$, suggests it as a suitable candidate for tremendous applications due to wide ranges of plasmon resonances from deep UV to the middle visible region [11].

The glancing angle deposition (GLAD) and

*Corresponding Author Email: m.gholizadeh.ar@gmail.com

oblique angle deposition (OAD) methods are usual to make porous thin films with controlled nanostructures. Non-isotropic structure of porous thin films [12, 13] causes tensional anisotropy and optical birefringence [14] and also affects their magnetic permeability [15]. The anisotropic degree is related to the element and substrate types and deposition angle [16]. Optically anisotropic thin films have a variety of applications including speed reduction optical plates [17], anisotropic antireflection coating [18], birefringent omnidirectional reflector [19], 3D photonic band gap crystals [20], birefringent thin film polarizers [21], new optical filters [14], polarization-selective mirrors and interferential filters [22]. Porous thin films had prepared with different structural properties, frequency filtering abilities and desired geometric shapes such as chiral, zig-zag and nano flowers and studied under the s- and p- polarized light irradiations [23-26, 28, 29].

RahChamani et al. prepared zig-zag nano-sculptured ZnS thin films by GLAD technique and showed that their refractive indexes are highly sensitive to the preparation conditions [23]. They also studied the optical properties of zig-zag nano-sculptured ZnS thin films with different growth angles at 10° and 70° incident light angles for both s- and p-polarized lights and showed their significant difference, indicating the employed angles were above Brewster's angle of ZnS film [24]. Liedtke et al. showed that the porosity is significantly influenced by the incident angle and substrate temperature [25]. There are many other issues on zig-zag thin film preparation by different methods [26-29].

The Bragg reflection is a phenomenon for creation of controllable optical filter components [30]. A variety of theoretical methods have been used to study the optical properties of porous thin films. The transition matrix is a useful method to determine the optical properties of anisotropic thin films by different morphologies. In this method, the structure of porous metal composite is homogenized by the Bruggeman formula to obtain the effective dielectric properties of the layers [31, 32]. The material-void fraction, material local direction and the layer thickness are the main parameters needed for the homogenization. Reduction of the electrical field amplitude in the anisotropic composite materials and high real scaler values of the metals electric permeability causes difficulties in the calculation of the reflection and transmission amplitudes, even for thick layers. To overcome these difficulties, the anisotropic material is usually considered as a semi-space structure, to obtain its reflection for vertical incident light [20].

Vepachedu, et. al prepared the ZnSe zig-zag structure of N=10 unit cells and compared the empirical and theoretical results of the Bragg phenomena for s- and p- linear polarized lights [33]. They did not observe the Bragg peaks in the zig-zag structures with the same arms lengths and 20° growth angle for the s- and p- polarized lights at different incident directions (θ) and zero azimuthal angle (ψ=0 °), but for ψ=90 ° and θ≳40 ° the Bragg peaks observed in a narrow spectral region.

This work is devoted to the study of linearly polarized light propagation in the Al zig-zag thin films, using transfer matrix method. At first, the Bragg phenomena of Al zig-zag thin films were simulated and studied for both s- and p- polarized incident light for different numbers of arms and incident light angles. The effects of nanostructure arm lengths on the Bragg phenomena were also investigated.

OPTICAL MODELING

The harmonic time dependency of the incident light is considered as $e\,\mathrm{xp}(i\omega t)$ which ω shows the angular frequency. The wave number, wavelength and intrinsic impedance of free space denoted by $k = \omega\sqrt{\varepsilon_0\mu_0}$, $\lambda = 2\pi/k$ and $\eta_0 = \sqrt{\varepsilon_0 / \mu_0}$, respectively. The μ_0 and ε_0 show the magnetic permeability and electrical permittivity of the free space, respectively. The Cartesian unit vectors

displayed by $\underline{u}_x$,$\underline{u}_y$, and $\underline{u}_z$. The vectors are underlined once and the dyadics underlined twice.

The studied model structure is a zig-zag thin film occupied the region 0 ≤ z ≤ d surrounded by vacuous regions z <0 and z >d as given in the Fig. 1. It is assumed that the structure is excited by a plane wave propagating with the incident angle θ to the z-axis and azimuthal angle ψ with the x-axis in the xy-plane. The phasors of incident, reflected and transmitted electric fields are given by [20]

$$\begin{cases} \underline{E}_{inc} = (a_s \underline{s} + a_p \underline{p}_+) e^{ik_0 z\cos\theta} \exp(i(kx\cos\psi + ky\sin\psi)) & z \le 0 \\ \underline{E}_{ref} = (r_s \underline{s} + r_p \underline{p}_-) e^{-ik_0 z\cos\theta} \exp(i(kx\cos\psi + ky\sin\psi)) & z \le 0 \\ \underline{E}_{tr} = (t_s \underline{s} + t_p \underline{p}_+) e^{ik_0 (z-L)\cos\theta} \exp(i(kx\cos\psi + ky\sin\psi)) & z \ge d \end{cases}$$

(1)

That is expressed in terms of the s- and p- polarized light components via the unit vectors

$$\begin{cases} \underline{s} = -\underline{u}_x \sin\psi + \underline{u}_y \cos\psi \\ \underline{p}_\pm = \mp(\underline{u}_x \cos\psi + \underline{u}_y \sin\psi)\cos\theta + \underline{u}_z \sin\theta \end{cases}$$

(2)

The parameters (a_s, a_p), (r_s, r_p) and (t_s, t_p) show the amplitudes of incident, reflected and transmitted waves, respectively with the s- and p- indexes as the linear polarization types. The phasor of the magnetic field in any region is given by $\underline{H} = (i\omega\mu_0)^{-1}\nabla \times \underline{E}$. We also have the following equations in the Cartesian coordinate system.

$$\begin{cases} \underline{r} = x\underline{u}_x + y\underline{u}_y + z\underline{u}_z \\ \underline{k}_0 = k_0\left(\sin\theta\cos\psi\,\underline{u}_x + \sin\theta\sin\psi\,\underline{u}_y + \cos\theta\,\underline{u}_z\right) \end{cases}$$

(3)

The continuity of the tangential components of the electrical and magnetic fields at the interfaces of thin films may be used to calculate the reflectance and transmittance amplitudes through the solution of the algebraic matrix equation

$$\begin{bmatrix} t_s \\ t_p \\ 0 \\ 0 \end{bmatrix} = \left[\underline{\underline{K}}(\theta,\psi)\right]^{-1} \cdot \left[\underline{\underline{M}}(d,k,\psi)\right] \cdot \left[\underline{\underline{K}}(\theta,\psi)\right] \cdot \begin{bmatrix} a_s \\ a_p \\ r_s \\ r_p \end{bmatrix}$$

(4)

The different terms and parameters of this equation are described in details, in the reference [20].

We now consider a zig-zag thin film with thickness of $d = Nt_z$, where t_z is the thickness of an arm of zig-zag, and N is the number of arms. The transfer matrix of a columnar thin film with thickness of t is given by $e^{i\left[\underline{\underline{P}}\right]t}$ [20]. Therefore, the transfer matrix of a zig-zag nanostructure is [23],

$$\left[\underline{\underline{M}}\right]_{zigzag} = \left[\underline{\underline{M}}\right]_N \left[\underline{\underline{M}}\right]_{N-1} \cdots \left[\underline{\underline{M}}\right]_2 \left[\underline{\underline{M}}\right]_1$$

(5)

Where $\left[\underline{\underline{M}}\right]_i = e^{i\left[\underline{\underline{P}}(\varsigma,\chi,\lambda_0,\theta,\psi)\right]t}$, $i = 1,2,...,N$.

The ζ and χ are the rotation angles of the arms about z-axis and the growth angle of columns to xy-plane, respectively. Replacing $\left[\underline{\underline{M}}(d,k,\psi)\right]$ by the transfer matrix of zig-zag, $\left[\underline{\underline{M}}\right]_{zigzag}$ in the Eq. (5), the reflectance and transmittance amplitudes may be calculated. The results in terms of the matrix relations are

$$\begin{bmatrix} r_s \\ r_p \end{bmatrix} = \begin{bmatrix} r_{ss} & r_{sp} \\ r_{ps} & r_{pp} \end{bmatrix} \begin{bmatrix} a_s \\ a_p \end{bmatrix}$$

(6)

And

$$\begin{bmatrix} t_s \\ t_p \end{bmatrix} = \begin{bmatrix} t_{ss} & t_{sp} \\ t_{ps} & t_{pp} \end{bmatrix} \begin{bmatrix} a_s \\ a_p \end{bmatrix}$$

(7)

Four reflection r_{xy} and transmission t_{xy} coefficients with x and y in {s, p} were used to compute the reflectance $R_{sp} = |r_{sp}|^2$, etc., and the

transmittances $T_{sp} = |t_{sp}|^2$, etc., of the zig-zag thin film.

Thin film is wholly dissipative, when the amplification is negligible. As a result, from the energy conservation principle, the inequalities must be hold.

$$\begin{cases} R_{ss} + R_{ps} + T_{ss} + T_{ps} < 1 \\ R_{pp} + R_{sp} + T_{pp} + T_{sp} < 1 \end{cases} \quad (8)$$

The optical absorption for s- and p-linear polarized lights are given by

$$A_i = 1 - \sum_{j=s,p} \left(R_{ji} + T_{ji} \right) \quad , \quad i = s, p \quad (9)$$

In order to model the optical characteristics of prepared sample, we considered a zig-zag structure for which relative permittivity scalars $\varepsilon_{a,b,c}$ may be calculated using the Bruggeman homogenization equations [31]. In this formalism, the two- component structure is composed of the Al metal and void. The relative permittivity scalars depend on different parameters, including geometric form factor, fraction of Al (f_{Al}), the wavelength in the free space and the refractive index. In addition, each column in the structure is considered as a string of identical long ellipsoids by small electrical interactions [31]. In all calculations, columnar form factors considered as

$$\left(\frac{c}{a}\right)_{Al} = \left(\frac{c}{a}\right)_{void} = 15, \left(\frac{b}{a}\right)_{Al} = \left(\frac{b}{a}\right)_{void} = 1 \quad (10)$$

That *c*, *a* and *b* are semi major axis and small half axes of ellipsoids, respectively [34]. We have used the bulk experimental refractive index of Al for homogenization [35]. In homogenization of the structure, effects of dispersion and dissipation of dielectric function are considered [36].

In order to investigate the optical properties of Al zig-zag thin film, the growth angle of columns was considered χ=30° and the void fraction were fixed at 0.85. For metallic fraction greater than 0.2, it is very difficult to observe the Bragg phenomena [37].

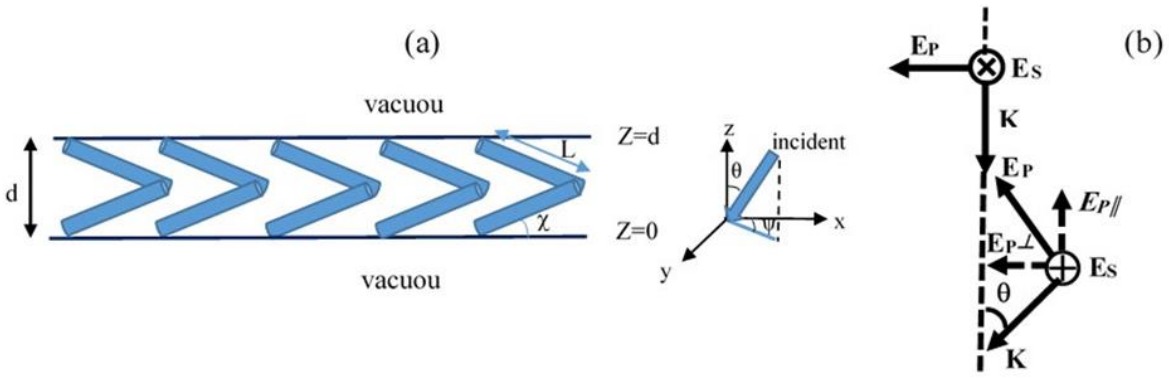

Fig. 1. Schematic representation of modeled zig-zag thin film.

RESULTS AND DISCUSSION

The effect of the arm number

The co-remittance spectra (i.e., Rpp, ss and Tpp, ss) of the Al zig-zag films with the arm numbers (2,4,8,16) at the 0° azimuthal angle and the incident light angles 0° , 30° , 60° and 80° are plotted in the Figures 2 to 5 for both s and p-polarized incident lights. Since, the cross-reflection and transmission spectra are very small compared to those obtained for the co-remittance spectra, the cross-remittance spectra are ignored [38]

Figure 2, shows the co-reflection Rpp, ss (Fig. 2a and 2b) and co-transmission Tpp, ss (Fig. 2c and 2d) spectra for the Al zig-zag film with 2 arms at azimuthal

angle ψ=0° and incident light angles θ = 0°, 30°, 60° and 80° for both s and p-polarized lights. According to the figure 2a and 2b, the co-reflection and co-transmission spectra for incident light angles θ = 0°, 30°, 60° and 80° for both s and p-polarized lights are opposite of each other. The Brewster angle of Aluminum thin-film at wavelength of 667 nm is 82° [39]. Therefore, for s-polarized incident light, the intensity of co-reflection spectrum (Fig. 2b) increases with incident angle, while the co-transmission spectrum (Fig. 2d) decreases.

The intensity of the co-reflection (co-transmission) for s-polarized light increases (decreases) with the incident light angle (θ) from 0° to 80° that may be devoted to more interaction of the electric field (Es) of the incident light with the structure surface. At azimuthal angles of 0°, the s- and p-polarized lights are perpendicular to each other, so the intensity of co-reflection (co-transmission) spectra for p-polarized light behaves opposite to the s-polarized light except at 80° that is near the Brewster angle. The intensity of co-reflection spectrum of p-polarized light decreases with the incident light angle, except at 80° that is near to the Brewster angle. Also, for the incident light angles 0° and 30°, three peaks can be observed at co-reflection spectrum of p-polarized light (Rpp) that shift towards lower wavelengths (blue shift), as the incident light angle increases. The behavior of co-transmission spectrum of p- polarized light (Tpp) for different incident light angles are almost the same.

The co-remittance spectra (i.e., Rpp, ss and Tpp, ss) for the Al zig-zag film with 4 arms at the azimuthal angle 0° and the incident light angles 0°, 30° , 60° and 80° for both s and p- polarized lights are shown in the Fig. 3. As the incident light angle increases, the intensity of the co-reflection (co-transmission) for s-polarized incident light increases (decreases) (Fig. 3a and 3b). The reflection spectra (Fig. 3b) of the s-polarized incident light for 60° and 80° incident angles have very wide peak at about 520 nm wavelength while transmission spectrum (Fig. 3d) has its minimum value. This may be considered as the beginning of the mirror Bragg phenomenon in these nanostructures. For the p-polarized incident light, and two arms, the behavior of transmission spectrum is the same at all incident angles. For the s-polarized incident light, as the incident light angle increases, except for the angles near the Brewster angle, the intensity of the co-reflection (co-transmission) decreases (increases). Also, in the reflection spectrum (Rpp) at the 0° and 30° incident angles, a peak is created in the wavelengths greater than 1000 nm that is out of assumed spectrum region. Increasing the incident angle to 60° and 80° creates a blue shift for the peak.

The co-remittance spectra (i.e., $R_{pp, ss}$ and $T_{pp, ss}$) for the Al zig-zag film with 8 arms (L=30 nm) at azimuthal angle 0° and incident light angles of 0° , 30° , 60° and 80° for both s and p- polarized lights are plotted in the Fig. 4. Increasing the incident light angle creates some peaks in the reflection spectrum of s-polarized incident light. In the reflection spectrum (Fig. 4b) for the incident angles of 60° and 80°, two peaks may be clearly observed in λ = 364 nm and $\lambda \gtrsim 900$ nm for which the transmission spectrum (Fig. 4d) has decreased. In other words, the mirror Bragg phenomenon occurs at these wavelengths that become more obvious by increasing the incident light angle. The behavior of co-remittance spectra for p-polarized incident light (i.e., R_{pp} and T_{pp}), are similar to the Al zig-zag film with 4 arms.

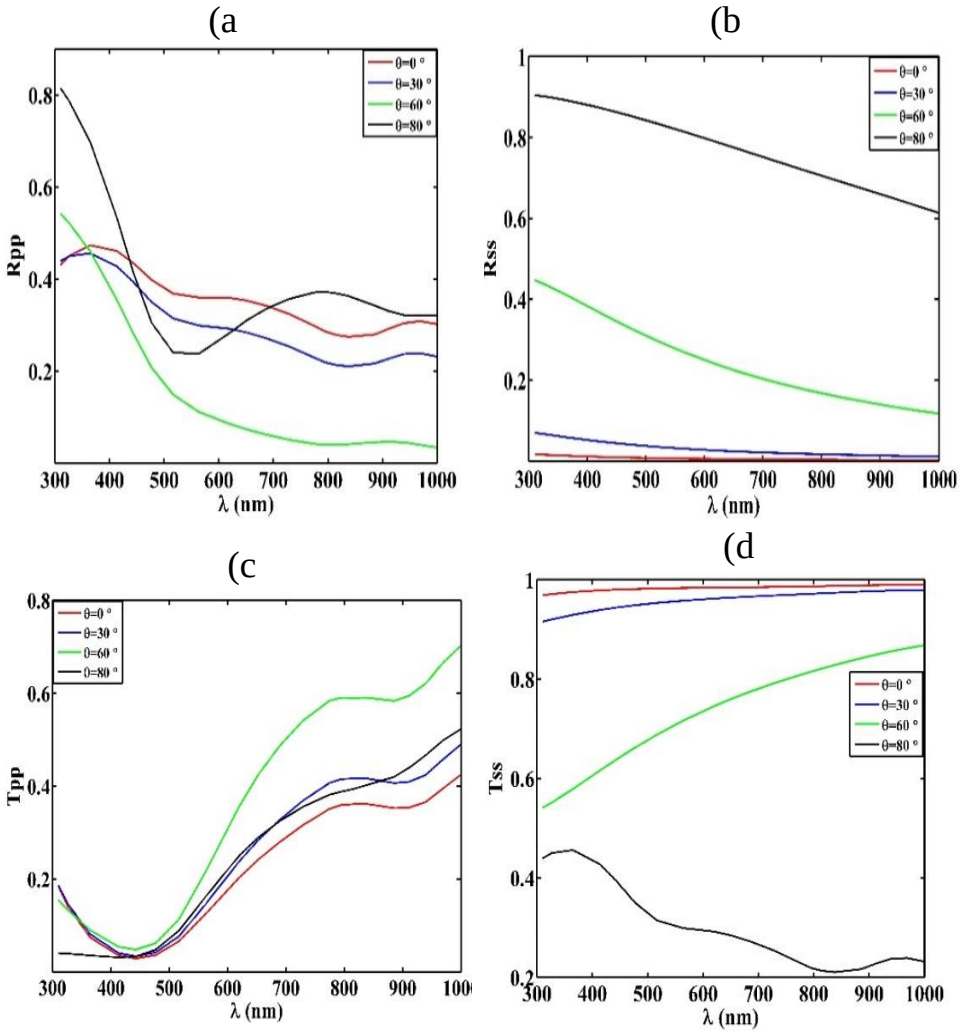

Fig. 2. Co-polarized reflectances $R_{ss,\,pp}$ and co-polarized transmittances $T_{ss,\,pp}$ spectra for both s- and p-polarized lights at incident light angles (θ = 0°, 30°, 60° and 80°) and azimuthal angle ψ=0° for Al zig-zag thin film with two arms

The co-remittance spectra (i.e., Rpp, ss and Tpp, ss) for the Al zig-zag film with 8 arms (L=30 nm) at azimuthal angle 0° and incident light angles of 0° , 30° , 60° and 80° for both s and p- polarized lights are plotted in the Fig. 4. Increasing the incident light angle creates some peaks in the reflection spectrum of s-polarized incident light. In the reflection spectrum (Fig. 4b) for the incident angles of 60° and 80°, two peaks may be clearly observed in λ = 364 nm and λ ≳900 nm for which the transmission spectrum (Fig. 4d) has decreased. In other words, the mirror Bragg phenomenon occurs at these wavelengths that become more obvious by increasing the incident light angle. The behavior of co-remittance spectra for p-polarized incident light (i.e., Rpp and Tpp), are similar to the Al zig-zag film with 4 arms. The co-remittance spectra (i.e., Rpp, ss and Tpp, ss) for the Al zig-zag film with 16 arms at azimuthal angle 0° and incident light angles 0° , 30° , 60° and 80° for both s and p-polarized lights are shown in the figure 5. Three peaks can be seen at λ= 300 nm, λ = 427 nm and λ= 730 nm for s-polarized incident light for which reflection spectra (Fig. 5b) are maximized and transmission spectra (Fig. 5d) reduced. As the incident light angle increases, the intensity of the mirror Bragg phenomenon increases, without any displacement of wavelengths. For the p- polarized incident light, as in the previous cases, no Bragg phenomenon was observed.

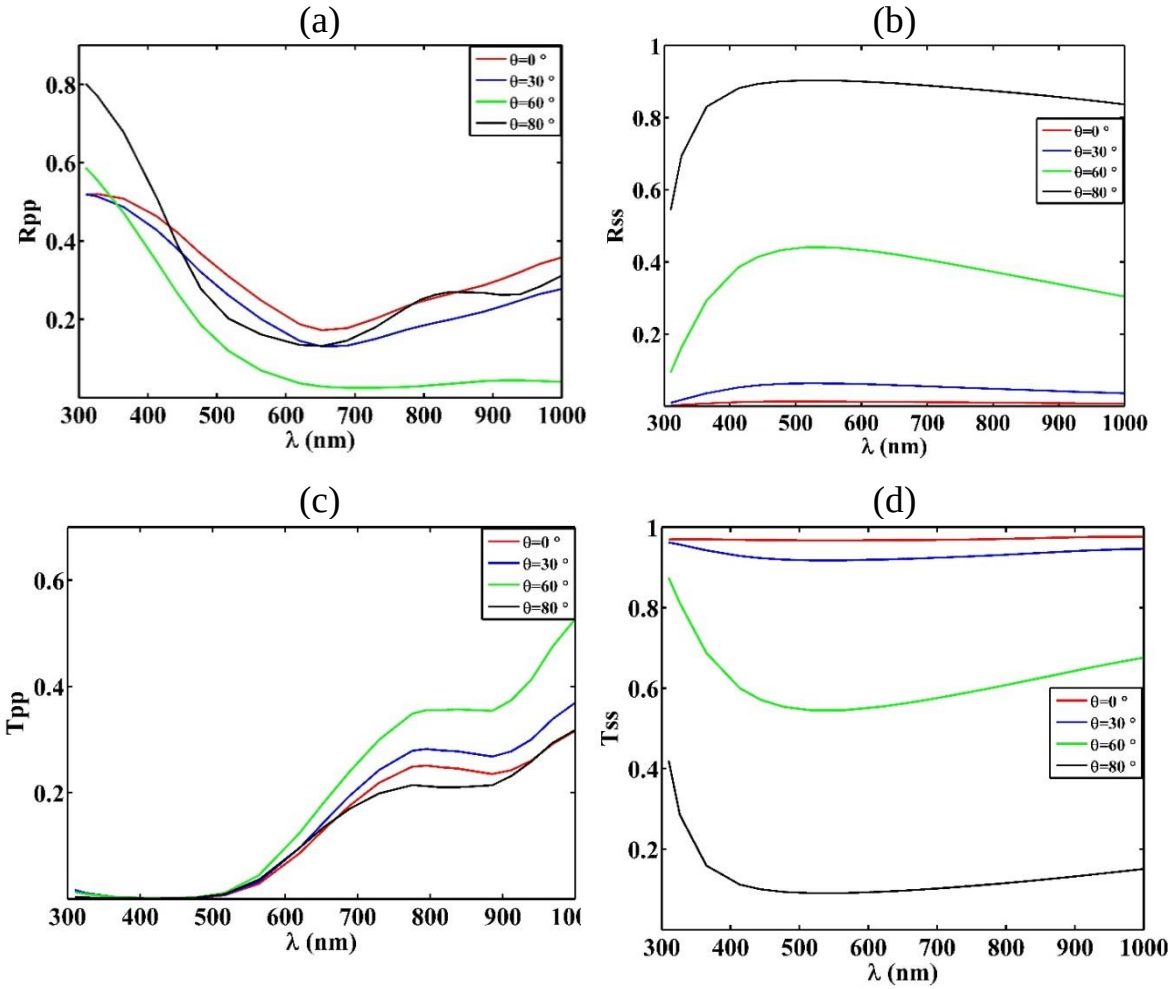

Fig. 3. Co-polarized reflectances $R_{ss,\ pp}$ and transmittances $T_{ss,\ pp}$ spectra for s- and p-polarized lights at θ = 0°, 30°, 60° and 80° incident light angles and azimuthal angle ψ=0° for Al zig-zag thin film with four arms.

The co-remittance spectra (i.e., Rss and Tss) for the Al zig-zag film with different numbers of arms (4,8,16) at the azimuthal angle 0° and incident light angle 60° for the light with s- polarized light are shown in the Fig 6. Since no Bragg phenomenon was observed for the Al zig-zag film with two arms, it was discarded. Also, at the incident light angle 60°, the Bragg peaks can be seen, clearly. The calculations were obtained for angle 60°, as it is close to the Brewster angle.

Since the Bragg peak depends on the period of structure, refractive index of the environment and incident light angle [40], in Al zig-zag film with 4, 8 and 16 arms there are 1, 2 and 3 Bragg peak, respectively, as shown in Fig. 6a. Accordingly, the structure period of Al zig-zag film is equal to four arms, and so for any 4 arms, a Bragg peak is created. Also, as the number of arms increases, the intensity of the peaks created in the reflectance spectrum remains constant and only the number of reflectance spectrum peaks increases. This behavior is not seen in the homogeneous and isotropic thin films.

Effects of arm lengths

Figure 7, shows the co-polarized reflectance Rss, pp (Fig. 7a and 7b) and co-polarized transmittance Tss, pp spectra (Fig. 7c and 7d) for both s and p-polarized light with the incident light angle θ = 60° and azimuthal angle ψ=0° for Al zig-zag thin films with 8 arms of different lengths (l=30, 60, 90, 120 nm).

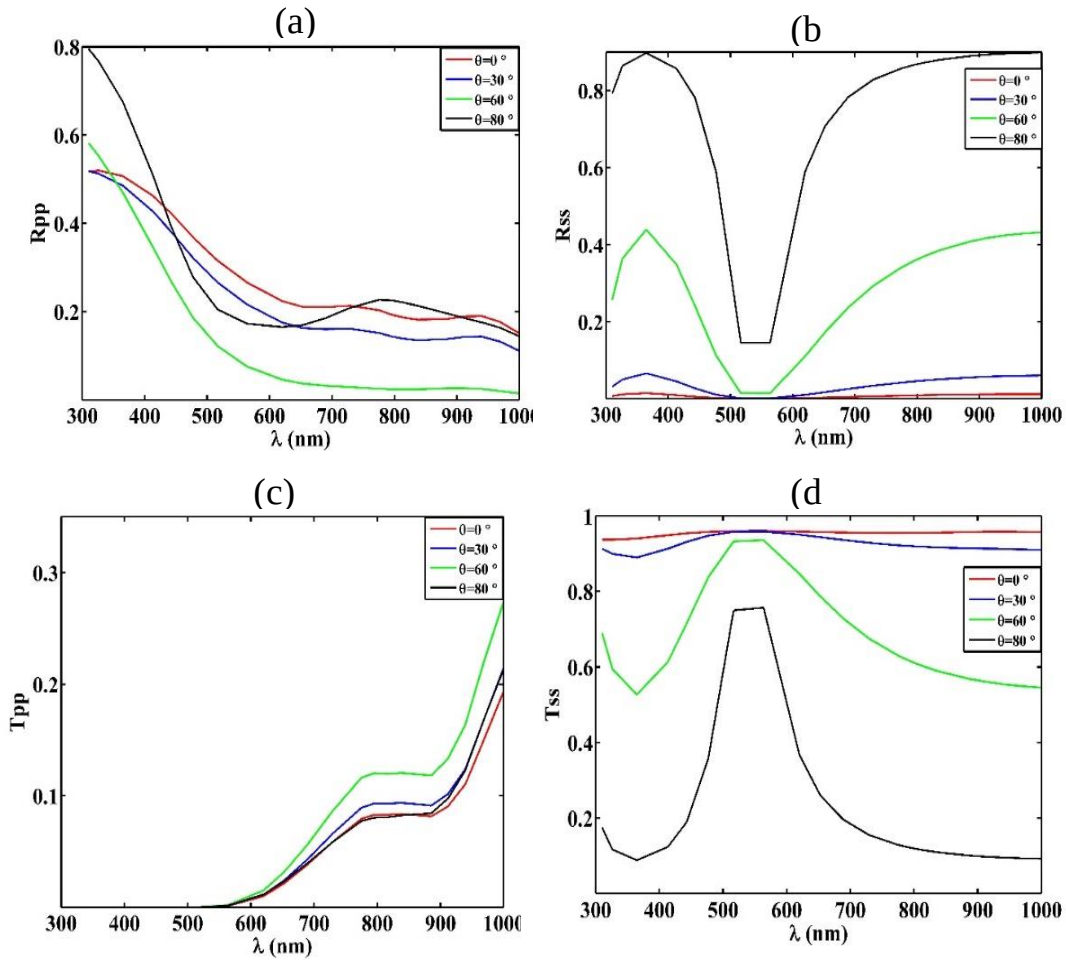

Fig. 4. Co-polarized reflectance Rss, pp and co-polarized transmittances Tss, pp spectra for both s- and p-polarized lights for different incident light angles (θ = 0°, 30°, 60° and 80°) and azimuthal angle ψ=0° for Al zig-zag thin film with 8 arms.

For p-polarized incident light, as the length of arms increased from 30 nm to 120 nm, no changes were observed in the reflectance spectrum behavior. The co-polarized reflectance spectrum (Rpp) was significantly reduced for $\lambda \rangle 600\, nm$. As the length of arms increases, the transmittance spectrum decreases. So, for Al zig-zag thin film with 8 arms and length of 120 nm, transmittance spectrum tends to zero. This may be devoted to the increase in layer thickness. Therefore, the p-polarized incident light is almost absorbed by the structure.

The Bragg peaks created in reflectance spectrum of s-polarizations incident light for the zig-zag nanostructure with 8 arms and different arm lengths are given in the Table 1. The red and blue shifts are shown with the arrows. For the s-polarization incident light, the number of the Bragg peaks had increased as arm length increased from 30 nm to 120 nm. At the arm length l = 30 nm, two peaks can be observed for $\lambda \rangle 364\, nm$ and $\lambda \sim 1000\, nm$. By increasing the arm length from 30 nm to 60 nm, two peaks are observed at $\lambda = 442\, nm$ and $\lambda = 792\, nm$, and simultaneously a peak begins to be appeared at $\lambda \sim 300\, nm$. Moreover, as the arm length increases, the peaks formed at low (long) wavelengths show red (blue) shift.

Simultaneously with increasing the arm length from 60 nm to 90 nm, three peaks are observed at $\lambda = 364\,nm$, $\lambda = 450\,nm$ and $\lambda = 650\,nm$. Besides, two peaks begin to be appeared in λ<300 nm and λ>1000 nm. Moreover, with increasing the arm length from 60 nm to 90 nm, the peaks formed in $\lambda\langle 300\,nm$ and $\lambda = 442\,nm$ have red shift to $\lambda = 364\,nm$ and $\lambda = 450\,nm$ respectively and the peak formed at $\lambda = 792\,nm$ has blue shift to $\lambda = 650\,nm$.

Also, with increasing the arm length from 90 nm to 120 nm, the peaks formed in $\lambda\langle 300\,nm$, $\lambda = 364\,nm$ and $\lambda = 450\,nm$ have red shift to $\lambda = 326nm$, $\lambda = 413\,nm$ and $\lambda = 476\,nm$, respectively while the peaks formed at $\lambda = 650\,nm$ and $\lambda\rangle 1000\,nm$ have blue shift to $\lambda = 619\,nm$ and $\lambda = 885\,nm$. It may be concluded that in the wavelengths about $\lambda = 550\,nm$, the wavelengths are divided into two groups similar to that seen in the spectrum of Tss and Rss.

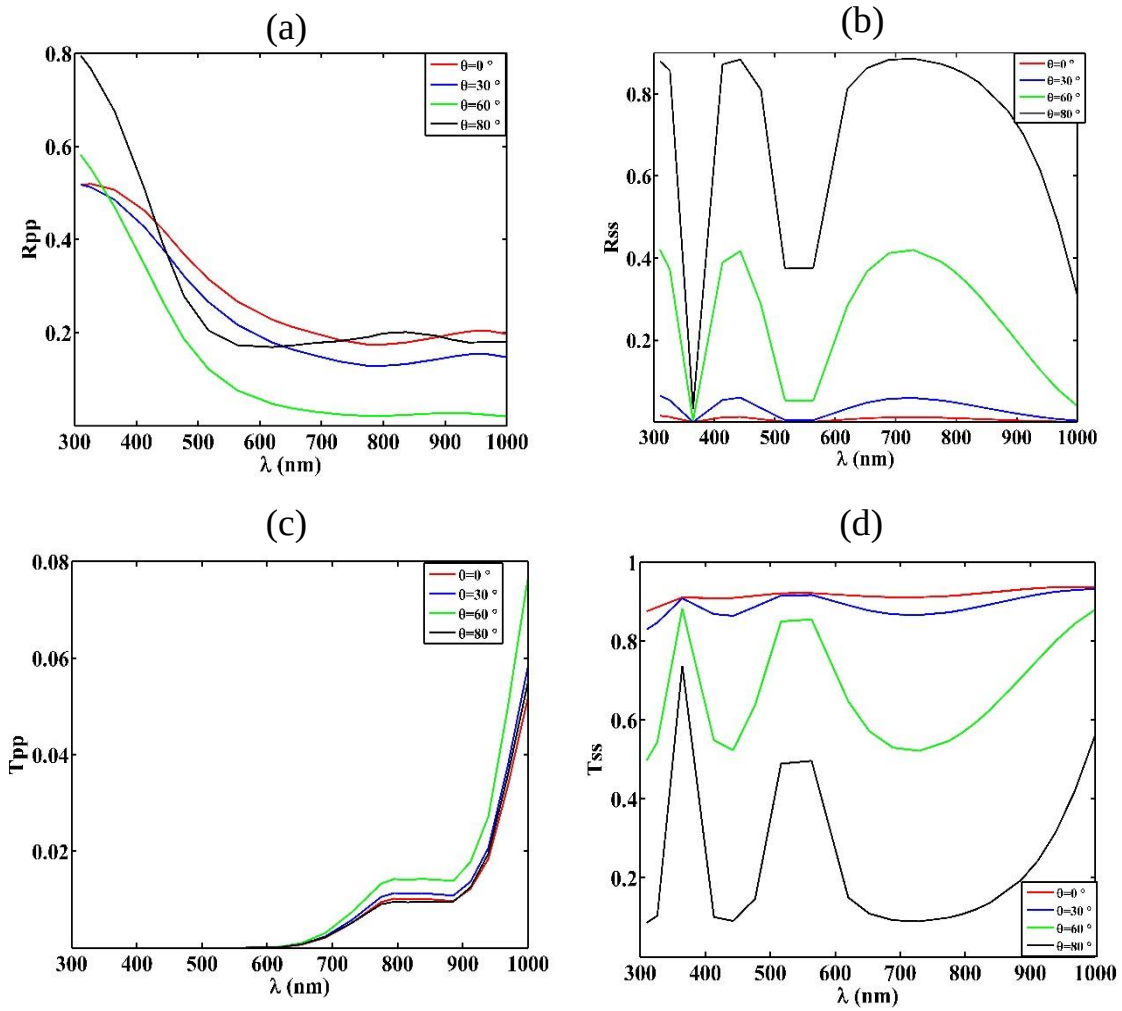

Fig. 5. Co-polarized reflectance Rss, pp and co-polarized transmittance Tss, pp spectra for s- and p- polarized lights at different incident angles (θ = 0°, 30°, 60° and 80°) at azimuthal angle ψ=0° for Al zig-zag thin film with 16 arms.

As the arm length increases, the peaks formed in the wavelengths shorter (longer) than 550 nm have red (blue) shift, respectively. Also, the number of peaks is increased for λ <300 nm and λ> 1000 nm. These behaviors can be seen for the nanostructures with 16 arms. But, because of the large number of peaks, their images are not shown. As a result, these nanostructures can be engineered by controlling the arm number and length and also incident light angle. CONCLUSION

The optical properties of aluminum nanostructures with zig-zag morphology were obtained using the transmission matrix method for linear s- and p-polarized incident lights. The reflection and transmission spectra of the zig-zag nanostructures with different arm numbers and lengths for both s- and p-polarized lights were obtained at different incident angles. The Bragg peaks begin to be appeared for zigzag nanostructures of more than 4 arms for s-polarized light at the angles greater than 30°. For zig-zag structures of 4, 8 and 16 arms, one, two and three Bragg peaks were observed, respectively. However, for p-polarized light, no Bragg peak was observed at any of the incident angles.

Also, for the zig-zag structure of 8 arms for s-polarized light at 60° the incident angles, the number of Bragg peaks are increased with increasing the arm length. In addition, the peaks created in the wavelengths below 550 nm showed red shift and the peaks appeared in the wavelengths above 550 nm showed blue shift.

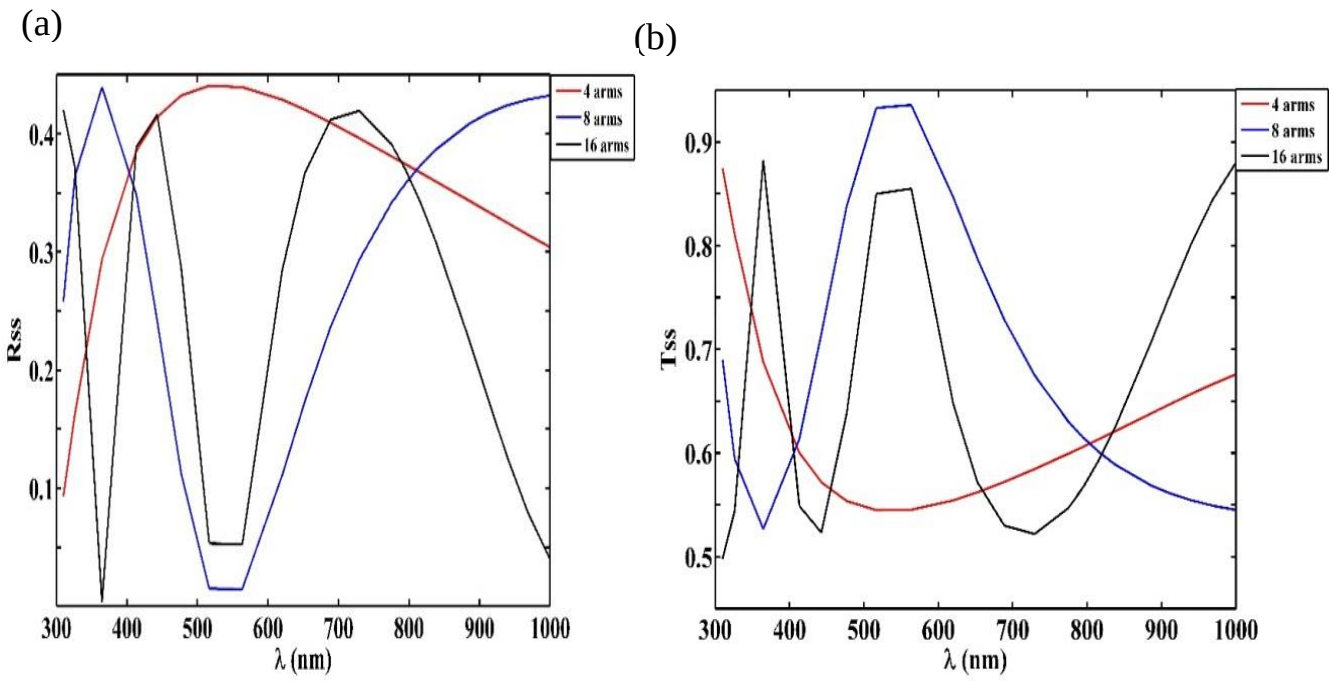

Fig. 6. The reflectance and transmittance spectra for s-polarized light at incident light angle θ = 60° and azimuthal angle ψ=0° for Al zig-zag thin film with different number of arms.

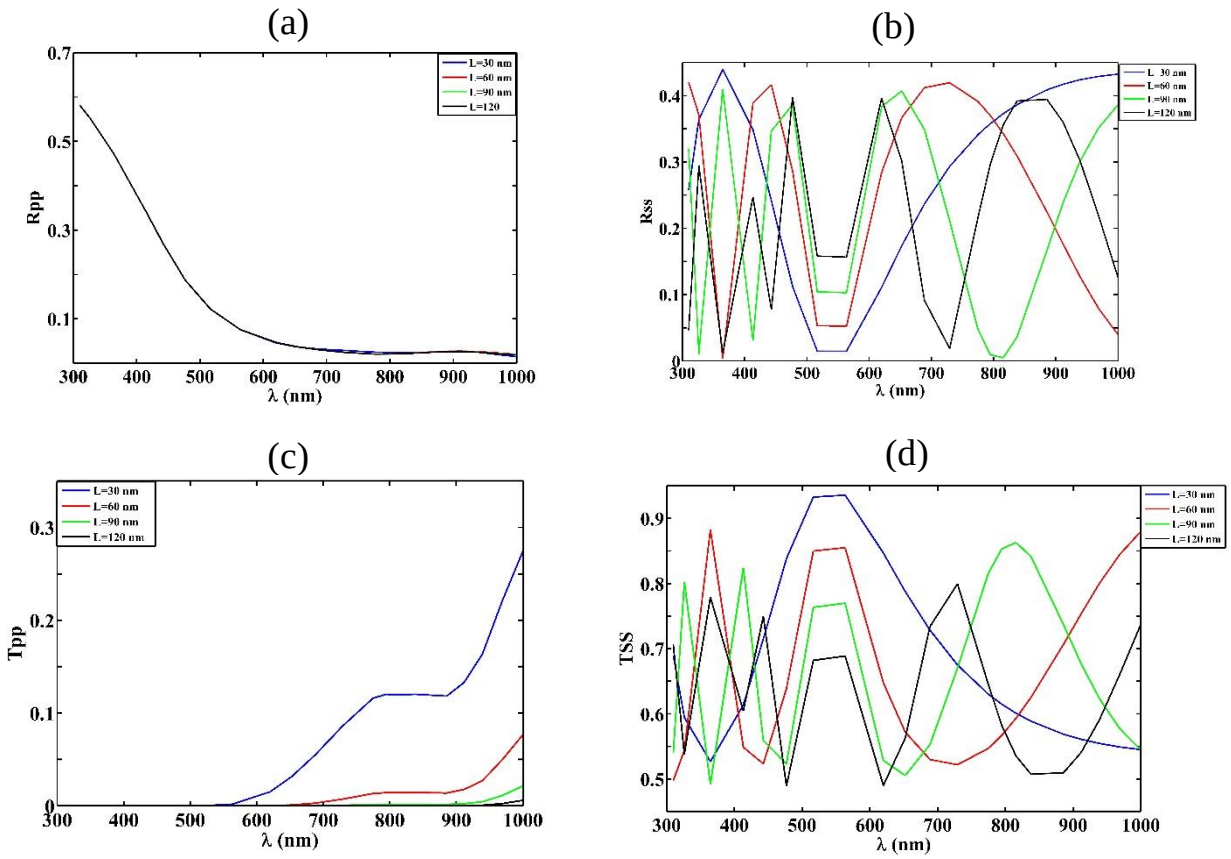

Fig. 7. Co-polarized reflectance $R_{ss,\,pp}$ and transmittance $T_{ss,\,pp}$ spectra of both s- and p-polarized lights at θ = 60° angle and azimuthal angle ψ=0° for Al zig-zag thin film with 8 arms of different lengths.

Table 1. The Bragg peaks created for s- polarized incident light for Al zig-zag thin film with 8 arms of different lengths.

L (nm)	λ_{Br} (nm)							
30	364	-	-	-	-	-	-	~1000
60	~300	442	-	-	-	-	792	-
90	< 300	364	450	-	-	650	> 1000	-
120	-	326	413	476	679	885	-	-

Simultaneously with increasing the arm length from 60 nm to 90 nm, three peaks are observed at $\lambda = 364\,nm$, $\lambda = 450\,nm$ and $\lambda = 650\,nm$. Besides, two peaks begin to be appeared in λ<300 nm and λ>1000 nm. Moreover, with increasing the arm length from 60 nm to 90 nm, the peaks formed in $\lambda\langle 300\,nm$ and $\lambda = 442\,nm$ have red shift to $\lambda = 364\,nm$ and $\lambda = 450\,nm$ respectively and the peak formed at $\lambda = 792\,nm$ has blue shift to $\lambda = 650\,nm$.

Also, with increasing the arm length from 90 nm to 120 nm, the peaks formed in $\lambda\langle 300\,nm$, $\lambda = 364\,nm$ and $\lambda = 450\,nm$ have red shift to

$\lambda = 326nm$, $\lambda = 413\,nm$ and $\lambda = 476\,nm$, respectively while the peaks formed at $\lambda = 650\,nm$ and $\lambda \rangle 1000\,nm$ have blue shift to $\lambda = 619\,nm$ and $\lambda = 885\,nm$. It may be concluded that in the wavelengths about $\lambda = 550\,nm$, the wavelengths are divided into two groups similar to that seen in the spectrum of T_{ss} and R_{ss}.

As the arm length increases, the peaks formed in the wavelengths shorter (longer) than 550 nm have red (blue) shift, respectively. Also, the number of peaks is increased for λ <300 nm and λ> 1000 nm. These behaviors can be seen for the nanostructures with 16 arms. But, because of the large number of peaks, their images are not shown. As a result, these nanostructures can be engineered by controlling the arm number and length and also incident light angle.

CONCLUSION

The optical properties of aluminum nanostructures with zig-zag morphology were obtained using the transmission matrix method for linear s- and p-polarized incident lights. The reflection and transmission spectra of the zig-zag nanostructures with different arm numbers and lengths for both s- and p-polarized lights were obtained at different incident angles. The Bragg peaks begin to be appeared for zigzag nanostructures of more than 4 arms for s- polarized light at the angles greater than 30°. For zig-zag structures of 4, 8 and 16 arms, one, two and three Bragg peaks were observed, respectively. However, for p-polarized light, no Bragg peak was observed at any of the incident angles.

Also, for the zig-zag structure of 8 arms for s-polarized light at 60° the incident angles, the number of Bragg peaks are increased with increasing the arm length. In addition, the peaks created in the wavelengths below 550 nm showed red shift and the peaks appeared in the wavelengths above 550 nm showed blue shift.

REFERENCES

[1] S. B. Mansoor, B. S. Yilbas, Opt. Laser Technol **101**, 107 (2018)

[2] G. Beck, S. Funk, Surf. Coat. Technol **206**, 2371 (2012)

[3] M. L. Green, R. A. Levy, R. G. Nuzzo, E. Coleman, Thin Solid Films **114**, 367 (1984)

[4] D. Vandembroucq, A. Tarrats, J. J. Greffet, S. Roux, F. Plouraboué, Opt. Commun **187**, 289 (2001)

[5] C. H. Cheung, A. B. Djuriši´c, C. Y. Kwong, H. L. Tam, K. W. Cheah, Z. T. Liu, W. K. Chan, P. C. Chui, J. Chan, A. D. Raki´c, Opt. Commun **248**, 287 (2005)

[6] D. Nieto, F. Cambronero, M. T. F. Arias, N. Farid, G. M. O'Conno , Optics and Lasers in Engineering **88** , 233 (2017)

[7] G. S. Rohrer, X. Liu, J. Liu, A. Darbal, M. N. Kelly, X. Chen, M. A. Berkson, N. T. Nuhfer, K. R. Coffey, K. Barmak, J. Mater. Sci **52**, 9819 (2017)

[8] C. S. Oh, J. S. Bae, S. H. Choa, H. J. Lee, Proceedings of the 13th International Conference on Experimental Mechanics, Alexandroupolis, Greece, Springer: Berlin, Germany,(2007)

[9] G. Kaune, E. Metwalli, R. Meier, V. Körstgens, K. Schlage, S. Couet, R. Röhlsberger, S. V. Roth, P. Müller-Buschbaum, ACS. Appl. Mater. Interfaces **3**, 1055 (2011)

[10] X. Yu-Qing, L. Xing-Cun, C. Qiang, L. Wen-Wen, Z. Qiao, S. Li-Jun, L. Zhong-Wei, W. Zheng-Duo, Y. Li-Zhen, Chin. Phys. B **21**, 78 (2012)

[11] A. Ziashahabi, R. Poursalehi, Materials Science **11**, 743 (2015)

[12] D. Vick, T. Smy, M. J. Brett, J. Mater. Res **17**, 2904 (2002)

[13] D. Vick, L. J. Friedrich, S. K. Dew, M. J. Brett, K. Robbie, M. Seto, Thin Solid Films **339**, 88 (1999)

[14] I. J. Hodgkinson , P. W. Wilson, Solid State Mater. Sci **15**, 27 (1988)

[15] H. Kranenburg, J. C. Lodder, Y. Maeda, L. Toth , J. A. Pompa, IEEE Trans. Magn **26**, 1620 (1990)

[16] K. Robbie, PhD Thesis (Alberta: University of

Alberta), (1998)

[17] T. Motohiro, Y. Taga, Appl. Opt **28**, 2466 (1989)

[18] J. Q. Xi, M. F. Schubert, J. K. Kim, E. F. Schubert, M. F. Chen, S. Y. Lin , Nat. Photon **1**, 176 (2007)

[19] K. Kaminska, K. Robbie, Appl. Opt **43,** 1570 (2004)

[20] A. Lakhtakia, R. Messier, Sculptured thin films: Nanoengineered Morphology and Optics, Vol. **122**, Bellingham, SPIE press, USA (2005)

[21] I. J. Hodgkinson , Q. H. Wu, Appl. Phys. Lett **74**, 1794 (1999)

[22] A. J. Mcphun, Q. H. Wu, I. J. Hodgkinson, Electron. Lett **34**, 360 (1998)

[23] S. Z. Rahchamani, H. R. Gholipour Dizjani, M. H. Ehsani, Applied Surface Science **356**, 1096 (2015)

[24] S. Z. Rahchamani, H. R. Gholipour Dizjani, M. H. Ehsani, Bull. Mater. Sci **40**, 897 (2017)

[25] Susann Liedtke, Christoph Grüner, Jürgen W. Gerlach and Bernd Rauschenbach, J. Nanotechnol **9**, 954 (2018)

[26] H. Savaloni, A. Esfandiar, Appl. Surf. Sci. **257**, 9425 (2011)

[27] F. Babaei, J. Mod. Opt **60**, 1370 (2013)

[28] S. A. Jewell, P. Vukusic and N.W. Roberts, N. J. Physics **9**, 99 (2007)

[29] P. Vukusic, R. Kelly, I. Hooper, J. R. Soc. Interface **6**, 193 (2009)

[30] M. Born, E. Wolf, Principles of Optics, 7th Ed. Cambridge University Press, Cambridge(1999)

[31] J. A. Sherwin, A. Lakhtakia, B. Michel, Opt. Commun **178**, 267 (2000)

[32] A. Lakhtakia, Mod. Simul. Mater. Sci. Eng **8**, 677 (2000)

[33] V. Vepachedu, P. D. McAtee, A. Lakhtakia, Journal of Nanophotonics **11**, 036018 (2017)

[34] J. A. Sherwin, A. Lakhtakia, I. J. Hodgkinson, Opt. Commun **209**, 369 (2002)

[35] E. D. Palik, Handbook of optical constants of solids. Academic press, NewYork, (1985).

[36] F. Babaei, J. Mod. Opt **58**,1292 (2011)

[37] F. Babaei, H. Savaloni, Opt. Commun **278**,321 (2007)

[38] B, Dick, M. J. Brett, T. Smy, J. Vac. Sci Technol B Microelectronics and Nanometer Structures Processing, Measurement, and Phenomena **21**, 21 (2003)

[39] K. M. McPeak, S. V. Jayanti, S. J. P. Kress, S. Meyer, S. Iotti, A. Rossinelli, and D. J. Norris, ACS Photonics **2**, 326 (2015)

[40] S. V. Kesapragada, P. Victor, O. Nalamasu, D. Gall, Nano Lett **6**, 854 (2006)